Quenching of Charge Transfer in Nitrobenzene Induced by Vibrational Motion

ARTICLE *in* JOURNAL OF PHYSICAL CHEMISTRY LETTERS · AUGUST 2015

Impact Factor: 7.46 · DOI: 10.1021/acs.jpclett.5b00990 · Source: PubMed

3 AUTHORS, INCLUDING:

Juan J. Nogueira

University of Vienna

15 PUBLICATIONS **81** CITATIONS

SEE PROFILE

Leticia González

University of Vienna

210 PUBLICATIONS **3,384** CITATIONS

SEE PROFILE

THE JOURNAL OF PHYSICAL CHEMISTRY Letters

Letter

pubs.acs.org/JPCL

Quenching of Charge Transfer in Nitrobenzene Induced by Vibrational Motion

J. Patrick Zobel, Juan J. Nogueira,* and Leticia González*

Institute of Theoretical Chemistry, University of Vienna, Währinger Straße 17, A-1090 Vienna, Austria

Supporting Information

ABSTRACT: Although nitrobenzene is the smallest nitro-aromatic molecule, the nature of its electronic structure is still unclear. Most notably, the lowest-energy absorption band was assessed in numerous studies providing conflicting results regarding its charge-transfer character. In this study, we employ a combination of molecular dynamics and quantum chemical methods to disentangle the nature of the lowest-energy absorption band of nitrobenzene. Surprisingly, the charge-transfer transition from the benzene moiety to the nitro group is found to be quenched by a flow of charge into the opposite direction induced by vibrational motion. Beyond clarifying the charge-transfer character of nitrobenzene, we show that the widely used approach of analyzing the ground-state minimum-energy geometry provides completely wrong conclusions.

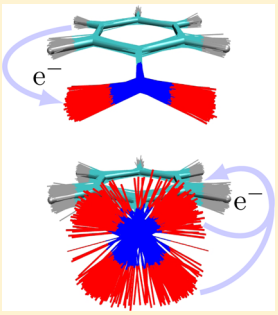

Nitrobenzene, despite having a simple structure, exhibits a rich and complex variety of reactive and nonreactive photoinduced events, including photodissociation[1−7] and ultrafast intersystem crossing.[8−10] In order to unravel the underlying mechanisms behind this rich photochemistry, it is of fundamental importance to properly characterize its molecular electronic excited states. Therefore, the electronic structure of nitrobenzene was widely investigated in the past by both experimental[11−18] and theoretical[18−21] techniques. Furthermore, nitrobenzene can be considered the smallest prototype of nitrated polycyclic aromatic hydrocarbons, a class of compounds that constitute an important type of widespread environmental pollutants with phototoxic effects, e.g., stimulating the formation of skin cancer.[22−24] Despite the large number of studies published until now, many features of the photophysics of nitrobenzene remain unclear. In particular, there is no consensus about the description of the charge-transfer (CT) character of the lowest-energy bright state of nitrobenzene obtained from different theoretical and experimental studies, indicating that the characterization of the excited states of this molecule is still a challenging task.

The gas-phase UV absorption spectrum of nitrobenzene is dominated by two strong bands centered at 240 and 193 nm.[11−13] The lowest-energy band has been assigned to a CT $\pi\pi^*$ excitation from the benzene ring to the nitro group on the basis of molecular orbital calculations as well as a solvent-induced red-shift of the absorption spectrum that becomes more pronounced with increasing solvent polarity.[12] Electro-optical absorption measurements of nitrobenzene in cyclohexane[14] and low-energy electron-impact excitation of solid films of nitrobenzene,[18] both supported by theoretical calculations, seconded the characterization as an intramolecular CT transition. A recent extensive study employing a wide range of quantum chemical methodologies backed this conclusion[21] despite showing large discrepancies in the energy of the CT state depending on the method employed. Intriguingly, the nature of the lowest-energy bright state has been addressed by polarization spectroscopy,[15,16] proposing that this state should be assigned mainly to a local excitation at the nitro group instead of a CT transition. This result is in sharp contrast to the characterization of the bright state obtained in the other studies. In passing, we mention that most conclusions extracted from all these studies, both experimental and theoretical, rely on the application of a C_{2v} symmetry restriction, which simplifies the interpretation of the results.

Motivated by the ambiguous findings of previous studies, we have computed and analyzed the absorption spectra of nitrobenzene in gas phase and aqueous solution by employing a combination of molecular dynamics simulations and quantum chemistry calculations. Our analyses show that the characterization of the electronic structure of nitrobenzene drastically changes if one considers the vibrational motion of the molecule. Thus, we are able to provide a completely different view from that obtained by examining only the ground-state minimum-energy geometry (S_0 geometry).

For simulating the absorption spectra of nitrobenzene in gas phase and aqueous solution, we used a sequential molecular mechanics/quantum mechanics approach (s-MM/QM).[25−27] Following this approach, first, a classical (MM) trajectory was computed for three different environments: both implicit and explicit aqueous solution as well as gas phase. Then, from each of the three trajectories 200 snapshots were selected at equidistant time intervals at which vertical excitation energies were calculated by means of a quantum mechanical (QM) approach (for gas phase), a hybrid quantum mechanics/molecular mechanics (QM/MM) approach (for explicit

Received: May 13, 2015
Accepted: July 13, 2015
Published: July 13, 2015

DOI: 10.1021/acs.jpclett.5b00990
J. Phys. Chem. Lett. 2015, 6, 3006−3011

solvation) and a quantum mechanics/polarizable-continuum model (QM/PCM) scheme (for implicit solvation). In all three scenarios, nitrobenzene is in the QM region and described with multistate complete-active-space second-order perturbation theory (MS-CASPT2).[28] Figure 1 shows the final spectra,

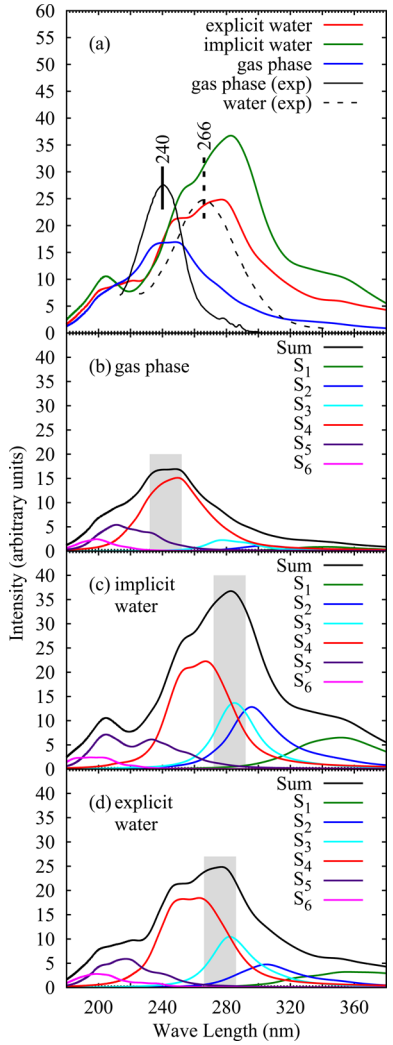

Figure 1. (a) Experimental (exp) UV absorption spectrum of nitrobenzene in gas phase (solid black line) and aqueous solution (dashed black line) taken from Nagakura et al.[12] s-MM/QM spectra computed in gas phase (blue), explicit water (red), and implicit water (green). The computed spectra (arbitrary units) are scaled so that the intensities of the experimental spectrum in aqueous solution and the computed spectrum in explicit water share the same maximum value. Calculated individual state contributions to the total absorption spectra in gas phase (b), implicit water (c), and explicit water (d). The gray areas indicate a 20 nm range around the band maxima employed in the identification of the character of the states (see text).

which were obtained through Lorentzian convolution of all calculated states for the 200 snapshots, and the experimental data.[12] Additionally, single-point vertical energies at the C_{2v} ground-state (S_0) geometry have been computed at the same MS-CASPT2 level of theory for the gas phase and implicit solution cases; the corresponding results are presented in Table 1. In the case of explicit aqueous solution, the calculation of the vertical energies at the S_0 geometry was not performed since the potential-energy surface presents a large number of energetically accessible minima and the arbitrary selection of one of these minima would provide a meaningless result. Additional computational details can be found in the Supporting Information (SI).

As can be seen in Figure 1a, the maxima of the experimental bands occur at 240 nm in the gas phase and at 266 nm in water. The computed bands center at 245 nm in gas phase and at 276 nm in explicit and 282 nm in implicit solvation, demonstrating a good agreement of the theoretical s-MM/QM and experimental absorption spectra. Both solvent models correctly reproduce the position of the band maximum, but the relative intensity with respect to gas phase is better described with the explicit solvent model. This is illustrated by integrating the absorption intensities between 220 and 360 nm for all curves and calculating the ratio between gas phase/water intensities for both solvent models and experiment. This ratio is 0.67 in the experiment, while it is 0.37 and 0.53 for implicit and explicit solvent models, respectively. The vertical excitation energy of the bright state S_4, computed applying C_{2v} symmetry at the S_0 geometry (cf. Table 1), is 243 nm in gas phase and 270 nm in implicit solution, thus also nicely matching the values of the experimental band maxima. The S_4 state is mainly described by the $\pi_2\pi_1^*$ configuration, with a contribution (c^2) of ca. 80%. Given the later good agreement with experiment, it is tempting to solely employ the S_0 geometry to characterize the excited states of nitrobenzene. However, an analysis of the state contributions to the absorption bands obtained from the s-MM/QM approach (Figures 1b–d), i.e., including vibrational sampling, reveals a very different physical picture from that based on the S_0 geometry, especially in solution.

The decomposition of the spectrum in gas phase (Figure 1b) shows that the absorption intensity is mainly due to the S_4 state, as could be expected from the large oscillator strength of S_4 at the S_0 geometry (cf. Table 1). In aqueous solution, the oscillator strength of the S_4 state is also by far the largest at the S_0 geometry. However, an inspection of the individual state contributions to the s-MM/QM bands (Figure 1c and 1d) reveals that in aqueous solution the S_1, S_2, and S_3 states add substantially to the absorption intensity of the spectrum, thus shifting the maximum of the absorption band to longer wave lengths. Note that the importance of the S_1–S_3 states could not have been predicted from the calculation based on the S_0 geometry. Most importantly, if only the S_0 geometry was considered, the solvatochromic red-shift of the absorption band would, erroneously, have been attributed solely to the eye-catching red-shift of the S_4 state from 243 to 270 nm, instead of to the participation of additional states.

The partitioning of the states in Figure 1 was performed based on energy criteria with states labeled according to increasing energy order. As an alternative description, we introduce a decomposition based on the character of the electronic states. Excited states characterized in such a way are often represented by their leading configuration for the sake of simplicity, as most states in Table 1. This simplification is, however, too crude for the majority of geometries obtained from the classical simulations because in most cases more than one configuration composes each electronic state. In order to account for this multiconfigurational nature, for each electronic state within a 20 nm range around the absorption maxima (highlighted in gray in Figure 1b–d), we examined the 10 leading configurations, which on average summed up to ~70% of the total wave function. An average contribution of a given configuration x, $\langle c_x^2 \rangle$, is then calculated as

DOI: 10.1021/acs.jpclett.5b00990
J. Phys. Chem. Lett. 2015, 6, 3006–3011

Table 1. Excited-State Properties of Nitrobenzene at the Ground-State Minimum-Energy C_{2v} Geometry (S_0 Geometry)

		gas phase			implicit water		
state	configuration	E^a	f^b	c^{2c}	E^a	f^b	c^{2c}
S_1 (A_2)	$n_1\pi_1^*$	337 (3.67)	0.000	69.9	352 (3.52)	0.000	70.6
S_2 (B_2)	$n_2\pi_1^*$	287 (4.32)	0.000	71.4	290 (4.28)	0.000	71.5
S_3 (B_1)	$\pi_1\pi_1^*$	273 (4.54)	0.003	31.1	286 (4.33)	0.003	31.7
	$\pi_2\pi_2^*$			28.1			25.9
S_4 (A_1)	$\pi_2\pi_1^*$	243 (5.10)	0.348	79.8	270 (4.60)	0.355	82.5
S_5 (B_1)	$\pi_3\pi_1^*$	208 (5.96)	0.025	45.1	215 (5.77)	0.031	43.5
S_6 (A_2)	$n_1\pi_3^*$	192 (6.45)	0.000	30.0	192 (6.45)	0.000	28.3
	$(n_1\pi_2)(\pi_1^*\pi_1^*)$			25.2			27.9

[a]Vertical excitation energy in nm (eV in parentheses). [b]Oscillator strengths in a.u. [c]Squared configuration-interaction coeffcients, representing the weights of the most important configurations (in percentage %).

Table 2. Average Excited-State Properties of an Ensemble of 200 Nitrobenzene Geometries

gas phase			implicit water			explicit water		
config.[a]	charge flow[b]	$\langle c^2\rangle^c$	config.[a]	charge flow[b]	$\langle c^2\rangle^c$	config.[a]	charge flow[b]	$\langle c^2\rangle^c$
$\pi_2\pi_1^*$	$CT_{R\to N}$	35.0	$\pi_2\pi_1^*$	$CT_{R\to N}$	24.4	$\pi_2\pi_1^*$	$CT_{R\to N}$	26.8
$(\pi_2\pi_2)(\pi_1^*\pi_1^*)$	$CT_{R\to N}$	5.1	$n_1\pi_1^*$	$CT_{N\to R}$	12.5	$n_1\pi_1^*$	$CT_{N\to R}$	9.7
$n_1\pi_1^*$	$CT_{N\to R}$	4.8	$n_2\pi_1^*$	$CT_{N\to R}$	9.2	$n_2\pi_1^*$	$CT_{N\to R}$	6.2
$\pi_3\pi_2^*$	LE	4.2	$\pi_2\pi_2^*$	LE	6.1	$\pi_2\pi_2^*$	LE	6.1
$(\pi_3\pi_3)(\pi_1^*\pi_1^*)$	LE	4.1	$\pi_1\pi_1^*$	$CT_{N\to R}$	6.1	$\pi_1\pi_1^*$	$CT_{N\to R}$	5.4
total charge flow[d]	$\langle c^2\rangle^c$		total charge flow[d]	$\langle c^2\rangle^c$		total charge flow[d]	$\langle c^2\rangle^c$	
Σ(LE)	13.0		Σ(LE)	12.5		Σ(LE)	13.2	
$\Sigma(CT_{R\to N})$	43.6		$\Sigma(CT_{R\to N})$	36.5		$\Sigma(CT_{R\to N})$	39.6	
$\Sigma(CT_{N\to R})$	10.7		$\Sigma(CT_{N\to R})$	25.6		$\Sigma(CT_{N\to R})$	19.3	
Net CT	32.9		Net CT	10.9		Net CT	20.3	
total $\langle c^2\rangle^e$	67.3		total $\langle c^2\rangle^e$	74.6		total $\langle c^2\rangle^e$	72.1	
$\langle\Delta\mu\rangle^f$	1.35		$\langle\Delta\mu\rangle^f$	0.83		$\langle\Delta\mu\rangle^f$	1.07	
$\langle\alpha\rangle^g$	42.8		$\langle\alpha\rangle^g$	42.4		$\langle\alpha\rangle^g$	42.3	

[a]Only the five leading configurations are reported. [b]Character of the corresponding configuration in terms of charge flow; LE: local excitation; $CT_{R\to N}$: benzene-ring-to-nitro-group charge transfer (CT); $CT_{N\to R}$: nitro-group-to-benzene-ring CT. [c]Averaged coefficient, cf. eq 1. [d]Sums (Σ) of all LE, $CT_{R\to N}$, and $CT_{N\to R}$; net CT character computed as $\Sigma(CT_{R\to N})$-$\Sigma(CT_{N\to R})$. [e]Contribution to the whole absorption band considering the first 10 leading configurations. [f]Averaged difference of the excited-state and ground-state dipole moments $\Delta\mu_i = \mu_i - \mu_0$ in Debye; averaging performed as $\langle\Delta\mu\rangle = (\sum_i\Delta\mu_i f_i)/(\sum_i f_i)$, where f_i is the oscillator strength of state Ψ_i. [g]Averaged angle $\langle\alpha\rangle$ between the transition dipole moment μ_{i0} and ground-state dipole moment μ_0 in degrees; averaging performed as $\langle\alpha\rangle = (\sum_i\alpha_i f_i)/(\sum_i f_i)$.

$$\langle c_x^2\rangle = \frac{\sum_i c_{xi}^2 f_i}{\sum_i f_i} \quad (1)$$

where the summation i runs over all the states Ψ_i contained within the 20 nm range, and each contribution is weighted by the oscillator strength f_i of the state it belongs to (see also SI for more details). The configurations with the five largest $\langle c_x^2\rangle$ coefficients are listed in Table 2, and the full list is given in Table S1 of the SI. In gas phase, the largest contribution (35.0%) to the absorption intensity corresponds to the $\pi_2\pi_1^*$ configuration, which is a CT transition from the benzene ring to the nitro group (see Figure 2a). This contribution is followed by a group of other configurations with smaller but non-negligible weights (ca. 5% versus 35%). In comparison, at the S_0 geometry (see Table 3), where only the S_4 state needs to be considered, a similar analysis shows that the $\pi_2\pi_1^*$ cofiguration also has the largest weight in the wave function (79.8%). However, in contrast to the ensemble, all other transitions are negligible in comparison to this one (ca. 1% versus 80%).

The difference in the relative weight of the leading $\pi_2\pi_1^*$ configuration with respect to the others, when comparing the S_0 geometry with the ensemble of geometries, is even more pronounced in aqueous solution. As can be seen in Table 2, in the ensemble, the $n_1\pi_1^*$ configuration has a weight of 12.5% in implicit water (9.7% in explicit water), which is ca. only half the weight of the $\pi_2\pi_1^*$ configuration of 24.4% in implicit water (26.8% in explicit water). In contrast, when only the S_0 geometry is considered (Table 3), the $\pi_2\pi_1^*$ configuration exhibits still by far the dominant contribution (82% versus 1%), similar to the gas phase situation. Thus, it becomes apparent

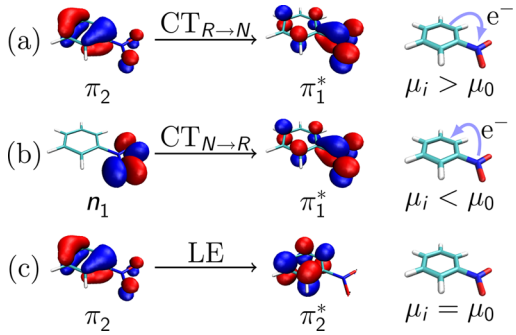

Figure 2. Example transitions for (a) benzene-ring-to-nitro-group charge transfer ($CT_{R\to N}$), (b) nitro-group-to-benzene-ring charge transfer ($CT_{N\to R}$), and (c) local excitations (LE). μ_i and μ_0 denote the excited-state and ground-state dipole moments, respectively.

DOI: 10.1021/acs.jpclett.5b00990
J. Phys. Chem. Lett. 2015, 6, 3006−3011

Table 3. Excited-State Contribution of the Bright S_4 State of Nitrobenzene at the C_{2v} S_0 Geometry

gas phase			implicit water		
config.[a]	charge flow[b]	c^{2c}	config.[a]	charge flow[b]	c^{2c}
$\pi_2\pi_1^*$	$CT_{R\rightarrow N}$	79.8	$\pi_2\pi_1^*$	$CT_{R\rightarrow N}$	82.5
$(\pi_1\pi_3)(\pi_1^*\pi_1^*)$	$CT_{R\rightarrow N}$	1.6	$(\pi_3\pi_3)(\pi_1^*\pi_1^*)$	LE	1.1
$\pi_1\pi_2^*$	LE	1.5	$(\pi_1\pi_1\pi_2)(\pi_1^*\pi_2^*\pi_2^*)$	LE	1.1
$(\pi_1\pi_1)(\pi_1^*\pi_1^*)$	$CT_{R\rightarrow N}$	1.2	$(\pi_1\pi_3)(\pi_1^*\pi_1^*)$	$CT_{R\rightarrow N}$	1.1
$\pi_4\pi_3^*$	LE	0.9	$(\pi_2\pi_4)(\pi_1^*\pi_1^*)$	$CT_{R\rightarrow N}$	0.9
total charge flow[d]		c^{2c}	total charge flow[d]		c^{2c}
Σ(LE)		2.9	Σ(LE)		3.2
$\Sigma(CT_{R\rightarrow N})$		85.2	$\Sigma(CT_{R\rightarrow N})$		86.1
$\Sigma(CT_{N\rightarrow R})$		0.0	$\Sigma(CT_{N\rightarrow R})$		1.3
Net CT		85.2	Net CT		84.8
Total c^{2e}		88.1	Total c^{2e}		90.6
$\Delta\mu^f$		6.52	$\Delta\mu^f$		7.84
α^g		0	α^g		0

[a]Only the five leading configurations are reported. [b]Character of the corresponding configuration in terms of charge flow; LE: local excitation; $CT_{R\rightarrow N}$: benzene-ring-to-nitro-group charge transfer (CT); $CT_{N\rightarrow R}$: nitro-group-to-benzene-ring CT. [c]Squared configuration-interaction coefficients, representing the weights of the most important configurations (in percentage %). [d]Sums (Σ) of all LE, $CT_{R\rightarrow N}$, and $CT_{N\rightarrow R}$; net CT character computed as $\Sigma(CT_{R\rightarrow N}) - \Sigma(CT_{N\rightarrow R})$. [e]Contribution to the S_4 state considering the first 10 leading configurations. [f]Difference of the excited S_4 state and ground-state dipole moment $\Delta\mu = \mu_4 - \mu_0$ in Debye. [g]Angle α between the transition dipole moment μ_{40} and ground-state dipole moment μ_0 in degrees.

that the solvatochromic effect of the absorption band observed when going from gas phase to water is partially induced by the admixture of $\pi_2\pi_1^*$ with additional configurations corresponding to the $S_1(n_1\pi_1^*)$, $S_2(n_2\pi_1^*)$, and $S_3(\pi_2\pi_2^*/\pi_1\pi_1^*)$ states at the S_0 geometry (see contributions c^2 of the leading configurations in Table 1). This demonstrates that the solvatochromic effect is not solely due to the red-shift of the $\pi_2\pi_1^*$ dominated CT excitation.

The admixture of the main $\pi_2\pi_1^*$ configuration with the $n\pi^*$ configurations due to nuclear motion (as discovered from the s-MM/QM calculations) has a major effect on the electronic charge flow during the excitation. In these $n\pi^*$ configurations, CT is directed from the nitro group to the benzene moiety, i.e., in the opposite direction as in the $\pi_2\pi_1^*$ configuration (compare Figure 2a,b). This means that the net CT character of the absorption band is drastically decreased by nuclear motion. This is best illustrated by calculating the difference between the excited-state and ground-state dipole moments $\Delta\mu_i = \mu_i - \mu_0$ as well as the angle α formed between the transition dipole moment μ_{i0} and ground-state dipole moment μ_0. $\Delta\mu$ is a direct measure of the amount of CT, and α describes the symmetry of the excitation (see SI for more details). These values are also reported in Tables 2 and 3.

The flow of charge from the benzene ring to the nitro group in the $\pi_2\pi_1^*$ configuration has the same direction as the ground-state dipole moment. This means that for a state dominated by the $\pi_2\pi_1^*$ electronic configuration, μ_i is larger than μ_0, and a large value of $\Delta\mu$ is expected (Figure 2a). Furthermore, in the idealized C_{2v} reference geometry the angle α must be 0°. This is because the $\pi_2\pi_1^*$ configuration is of A_1 symmetry and, thus, its transition dipole moment is parallel to the C_2 symmetry axis of the nitrobenzene molecule, as is the ground-state dipole moment. Precisely this is obtained for nitrobenzene at the S_0 geometry due to the planar structure: $\Delta\mu$ presents large values of 6.52 and 7.84 D in gas phase and water, respectively, and α obviously is 0° (Table 3). This picture changes completely when nuclear motion is switched on and an ensemble of geometries around the S_0 geometry is considered. The s-MM/QM simulations (Table 2) show that the angle α increases to ~42° in both gas phase and aqueous solution because configurations corresponding to excited states with transition dipole moment perpendicular to the ground-state dipole moment become important. This angle of ~42° is much closer to the value of 67°, derived in gas phase from polarization spectroscopy experiments.[15,16] Furthermore, the excited-state dipole moments substantially decrease, and thus $\Delta\mu$ shows values of 1.35 D (gas phase), 0.83 D (implicit solution) and 1.07 D (explicit solution). The previous analysis clearly indicates that the vibrational motion of the molecule quenches the CT character of the absorption band by diminishing the $\pi_2\pi_1^*$ contribution and inducing perpendicular electronic transitions.

In order to quantify the CT character of the lowest-energy absorption band of nitrobenzene, it is useful to classify the 10 leading configurations considered earlier according to their character. To this end, the total contribution of different types of configurations corresponding to local excitations (LE), ring-to-nitro-group charge-transfer ($CT_{R\rightarrow N}$) transitions, and nitro-group-to-ring charge-transfer ($CT_{N\rightarrow R}$) transitions to the total absorption band are also listed in Tables 2 and 3 for the s-MM/QM and S_0 geometries, respectively. Example transitions of each kind are depicted in Figure 2. The net amount of CT from the benzene ring to the nitro group is defined as the difference between the contributions of $CT_{R\rightarrow N}$-type and $CT_{N\rightarrow R}$-type configurations. This net CT at the S_0 geometry is ~85% in both gas phase and aqueous solution, while it decreases to 33% (gas phase), 11% (implicit water), and 20% (explicit water) for the ensemble of geometries, definitively proving that CT is quenched by molecular vibration. Attending only to the values of $\Delta\mu$, the S_0 geometry-based analysis predicts an erroneously increase of CT when going from gas phase (6.52 D) to aqueous solution (7.84 D). The correct behavior is observed in the s-MM/QM analysis with $\Delta\mu$ values of 1.35 D in gas phase and 0.83 D as well as 1.07 D in implicit and explicit solvent, respectively. The latter numbers also show that the nitrobenzene/water electrostatic interactions lead to a further decrease of CT character, especially in the implicit solution case, with $n\pi^*$ contributions larger than those in the explicit

DOI: 10.1021/acs.jpclett.5b00990
J. Phys. Chem. Lett. 2015, 6, 3006−3011

solution model (Table 2). In view of the better agreement of the explicit versus implicit solvent model with the experimental spectra (Figure 1a), the description of the CT character should be more realistic in the former one.

The vibrational motion responsible for the quenching of the CT character is analyzed in Figure 3a which displays a

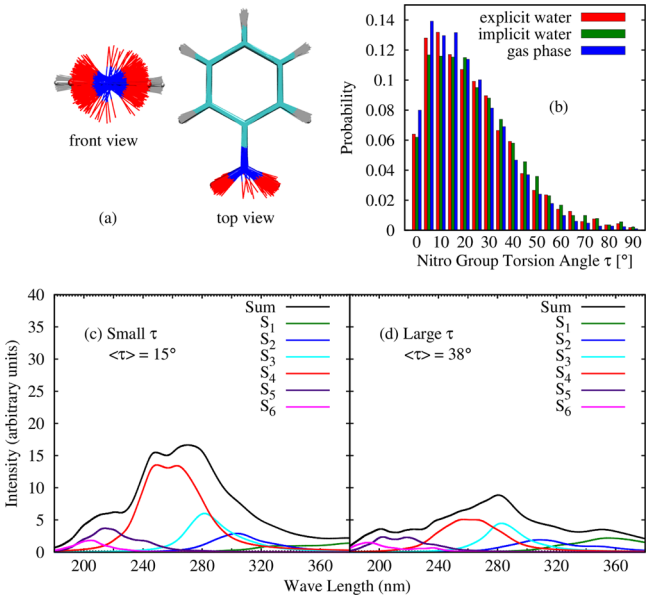

Figure 3. (a) Superposition of the 200 structures employed in the calculation of the absorption spectra in explicit water. (b) Probability distribution of nitro group torsion angles along the classical MD simulation. Calculated absorption spectrum of nitrobenzene in explicit solution for the 100 snapshots with the smallest (c) and largest (d) torsional angles τ. $\langle\tau\rangle$ denotes the average torsional angle.

superposition of the 200 nitrobenzene molecules selected from the s-MM/QM calculations. It is apparent that the largest deviation from the planar S_0 geometry corresponds to the torsional rotation of the nitro group, while the atoms of the ring nearly stay in the same plane. The torsional angle distribution of the nitro group depicted in Figure 3b shows a most probable angle of 15° and an average angle of 23°—values very different from 0°, as used in simplified models restricted to C_{2v} symmetry. In order to corroborate that the torsion of the nitro group is responsible for the quenching of the CT character, the absorption spectra for the 100 snapshots with the smallest and the largest torsional angles, respectively, are plotted in Figure 3c–d in explicit solution (gas phase and implicit solution spectra are in Figure S3 of SI). It is clear that the S_4 state, whose main configuration is $\pi_2\pi_1^*$, dominates the absorption band for geometries with small torsional angles (close to the S_0 geometry) but it does not for large torsional angles. In order to analyze the role of hydrogen bonding, the absorption spectrum in explicit solution was computed for geometries with and without the presence of hydrogen bonds between nitrobenzene and water, but no significant differences were found (not shown).

Summarizing, the absorption spectrum of nitrobenzene in both gas phase and aqueous solution has been investigated combining classical molecular dynamics simulations with high-level quantum chemical methodologies. This approach, allowing one to sample a number of geometries around the ground-state minimum-energy geometry, provides for the first time a clear picture of the excited-state character of the lowest energy absorption band of nitrobenzene, in very good agreement with experimental results. We analyzed the state compositions around the maxima of the absorption bands and found that the torsional motion of the nitro group induces a change in the composition of the states describing the absorption band. Compared to the static picture obtained at the C_{2v} S_0 geometry, where the CT transition from the benzene ring to the nitro group dominates, the absorption band in the ensemble has additional contributions from configurations with charge flow in the opposite direction. These opposing CT contributions result in a drastic lowering of the net CT of the absorption band in gas phase—an effect that is even more pronounced in aqueous solution. Comparison of explicit and implicit solvent results reveals that the implicit model overestimates the contribution of $n\pi^*$ configurations. The decrease of the net CT in all ensembles is in clear contradiction to the results obtained from the analysis of the rigid C_{2v} S_0 geometry, in which the net CT is very large in both gas phase and aqueous solution. We have therefore shown that a correct interpretation of the electronic structure of nitrobenzene is only achieved by considering an ensemble of geometries that accounts for the vibrational motion. Our results show that the effect of vibrational motion should be investigated in the excited states of other nitro aromatic compounds.

■ ASSOCIATED CONTENT

Supporting Information

Complete computational details along with the orbitals comprising the active space (Figure S1), contributions of the leading configurations (Table S1), coordinates of optimized structures (Table S2), superpositions of structures employed in the QM and QM/PCM calculations (Figure S2), and the individual state contributions to the absorption spectrum distinguished by the nitro group torsional angle for gas phase and solution (Figure S3) are given in the Supporting Information. The Supporting Information is available free of charge on the ACS Publications website at DOI: 10.1021/acs.jpclett.5b00990.

■ AUTHOR INFORMATION

Corresponding Authors

*E-mail: nogueira.perez.juanjose@univie.ac.at.
*E-mail: leticia.gonzalez@univie.ac.at.

Notes

The authors declare no competing financial interest.

■ ACKNOWLEDGMENTS

J.P.Z. is a recipient of a DOC Fellowship of the Austrian Academy of Sciences at the Institute of Theoretical Chemistry at the University of Vienna. The computational results presented have been partially achieved using the Vienna Scientific Cluster (VSC).

■ REFERENCES

(1) Galloway, D. B.; Bartz, J. A.; Huey, L. G.; Crim, F. F. Pathways and Kinetic Energy Disposal in the Photodissociation of Nitrobenzene. *J. Chem. Phys.* **1993**, *98*, 2107–2114.
(2) Li, Y.-M.; Sun, J.-L.; Yin, H.-M.; Han, K.-L.; He, G.-Z. Photodissociation of Nitrobenzene at 266 nm: Experimental and Theoretical Approach. *J. Chem. Phys.* **2003**, *118*, 6244–6249.

DOI: 10.1021/acs.jpclett.5b00990
J. Phys. Chem. Lett. 2015, 6, 3006–3011

(3) Yang, R.; Jin, X.; Wang, W.; Fan, K.; Zhou, M. Infrared Spectra of Phenyl Nitrite and Phenoxyl Radical-Nitric Oxide Complex in Solid Argon. *J. Phys. Chem. A* **2005**, *109*, 4261−4266.
(4) Zhu, X.-M.; Zhang, S.-Q.; Zheng, X.; Phillips, D. L. Resonance Raman Study of Short-Time Photodissociation Dynamics of the Charge-Transfer Band Absorption of Nitrobenzene in Cyclohexane Solution. *J. Phys. Chem. A* **2005**, *109*, 3086−3093.
(5) He, Y.; Gahlmann, A.; Feenstra, J. S.; Park, S. T.; Zewail, A. H. Ultrafast Electron Diffraction: Structural Dynamics of Molecular Rearrangement in the NO Release from Nitrobenzene. *Chem. - Asian J.* **2006**, *1*, 56−63.
(6) Lin, M.-F.; Lee, Y. T.; Ni, C.-K.; Xu, S.; Lin, M. C. Photodissociation Dynamics of Nitrobenzene and o-Nitrotoluene. *J. Chem. Phys.* **2007**, *126*, 064310.
(7) Hause, M. L.; Herath, N.; Zhu, R.; Lin, M. C.; Suits, A. G. Roaming-Mediated Isomerization in the Photodissociation of Nitrobenzene. *Nat. Chem.* **2011**, *3*, 932−937.
(8) Yip, R. W.; Sharma, D. K.; Giasson, R.; Gravel, D. Picosecond Excited-State Absorption of Alkyl Nitrobenzenes in Solution. *J. Phys. Chem.* **1984**, *88*, 5770−5772.
(9) Takezaki, M.; Hirota, N.; Terazima, M. Nonradiative Relaxation Processes and Electronic Excited States of Nitrobenzene Studied by Picosecond Time-Resolved Transient Grating Method. *J. Phys. Chem. A* **1997**, *101*, 3443−3448.
(10) Takezaki, M.; Hirota, N.; Terazima, M. Relaxation of Nitrobenzene from the Excited Singlet State. *J. Chem. Phys.* **1998**, *108*, 4685−4686.
(11) Hastings, S. H.; Matsen, F. A. The Photodecompositon of Nitrobenzene. *J. Am. Chem. Soc.* **1948**, *70*, 3514−3515.
(12) Nagakura, S.; Kojima, M.; Maruyama, Y. Electronic Spectra and Electronic Structures of Nitrobenzene and Nitromesitylene. *J. Mol. Spectrosc.* **1964**, *13*, 174−192.
(13) Vidal, B.; Murrell, J. N. The Effect of Solvent on the Position of the First Absorption Band of Nitrobenzene. *Chem. Phys. Lett.* **1975**, *31*, 46−47.
(14) Sinha, H. K.; Yates, K. Ground- and Excited-Statet Dipole Moments of some Nitroaromatics: Evidence for Extensive Charge-Transferr in Twisted Nitrobenzene Systems. *J. Chem. Phys.* **1990**, *93*, 7085−7093.
(15) Castle, K. J.; Abbott, J. E.; Peng, X.; Kong, W. Direction of the Transition Dipole Moment of Nitrobenzene Determined From Oriented Molecules in a Uniform Electric Field. *J. Chem. Phys.* **2000**, *113*, 1415−1419.
(16) Abbott, J. E.; Peng, X.; Kong, W. Symmetry Properties of Electronically Excited States of Nitroaromatic Compounds. *J. Chem. Phys.* **2002**, *117*, 8670−8675.
(17) Kawski, A.; Kukliński, B.; Bojarski, P. Excited S_1 State Dipole Moments of Nitrobenzene and *p*-Nitroaniline from Thermochromic Effect on Electronic Absorption Spectra. *Chem. Phys.* **2006**, *330*, 307−312.
(18) Kröhl, O.; Malsch, K.; Swiderek, P. The Electronic States of Nitrobenzene: Electron-Energy-Loss Spectroscopy and CASPT2 Calculations. *Phys. Chem. Chem. Phys.* **2000**, *2*, 947−953.
(19) Takezaki, M.; Hirota, N.; Terazima, M.; Sato, H.; Nakajima, T.; Kato, S. Geometries and Energies of Nitrobenzene Studied by CAS-SCF calculations. *J. Phys. Chem. A* **1997**, *101*, 5190−5195.
(20) Quenneville, J.; Greenfield, M.; Moore, D. S.; McGrane, S. D.; Scharff, R. J. Quantum Chemistry Studies of Electronically Excited Nitrobenzene, TNA, and TNT. *J. Phys. Chem. A* **2011**, *115*, 12286−12297.
(21) Mewes, J.-M.; Jovanović, V.; Marian, C. M.; Dreuw, A. On the Molecular Mechanism of Non-Radiative Decay of Nitrobenzene and the Unforeseen Challenges this Simple Molecule Holds for Electronic Structure Theory. *Phys. Chem. Chem. Phys.* **2014**, *16*, 12393−12406.
(22) Yu, H. Environmental Carcinogenic Polycyclic Aromatic Hydrocarbons: Photochemistry and Phototoxicity. *J. Environ. Sci. Health C* **2002**, *20*, 149−183.
(23) Fu, P. P.; Xia, Q.; Sun, X.; Yu, H. Phototoxicity and Environmental Tranformation of Polycyclic Aromatic Hydrocarbons (PAHs) - Light-Induced Reactive Oxygen Species, Lipid Peroxidation, and DNA Damage. *J. Environ. Sci. Health C* **2012**, *30*, 1−41.
(24) Xia, Q.; Yin, J. J.; Zhao, Y.; Wu, Y. S.; Wang, Y. Q.; Ma, L.; Chen, S.; Sun, X.; Fu, P. P.; Yu, H. UVA Photoirradiation of Nitro-Polycyclic Aromatic Hydrocarbons - Induction of Reactive Oxygen Species and Formation of Lipid Peroxides. *Int. J. Environ. Res. Public Health* **2013**, *10*, 1062−1084.
(25) Coutinho, K.; Canuto, S.; Zerner, M. C. A Monte Carlo-Quantum Mechanics Study of the Solvatochromic Shifts of the Lowest Transition of Benzene. *J. Chem. Phys.* **2000**, *112*, 9874−9880.
(26) Röhrig, U. F.; Frank, I.; Hutter, J.; Laio, A.; van de Vondele, J.; Rothlisberger, U. QM/MM Car-Parrinello Molecular Dynamics Study of the Solvent Effects on the Ground State and on the First Excited Singlet State of Acetone in Water. *ChemPhysChem* **2003**, *4*, 1177−1182.
(27) Besley, N. A.; Oakley, M. T.; Cowan, A. J.; Hirst, J. D. A Sequential Molecular Mechanics/Quantum Mechanics Study of the Electronic Spectra of Amides. *J. Am. Chem. Soc.* **2004**, *126*, 13502−13511.
(28) Finley, J.; Malmqvist, P.-Å; Roos, B. J.; Serrano-Andrés, L. The Multi-State CASPT2 Method. *Chem. Phys. Lett.* **1998**, *288*, 299−306.

DOI: 10.1021/acs.jpclett.5b00990
J. Phys. Chem. Lett. 2015, 6, 3006−3011